J. Fluid Mech. (2000), *vol.* 413, *pp.* 355–378. Printed in the United Kingdom

Nonlinear instability of a contact line driven by gravity

By SERAFIM KALLIADASIS

Department of Chemical Engineering, University of Leeds, Leeds LS2 9JT, UK

(Received 25 November 1998 and in revised form 24 June 1999)

A thin liquid mass of fixed volume spreading under the action of gravity on an inclined plane develops a fingering instability at the front. In this study we consider the motion of a viscous sheet down a pre-wetted plane with a large inclination angle. We demonstrate that the instability is a phase instability associated with the translational invariance of the system in the direction of flow and we analyse the weakly nonlinear regime of the instability by utilizing methods from dynamical systems theory. It is shown that the evolution of the fingers is governed by a Kuramoto–Sivashinsky-type partial differential equation with solution a saw-tooth pattern when the inclined plane is pre-wetted with a thin film, while the presence of a thick film suppresses fingering.

1. Introduction

A key feature of numerous technological applications, in particular thin liquid film coating, is dynamic wetting, that is the displacement of a gas by a liquid on a solid surface. Central to any description of wetting is the dynamic contact line problem which includes the stress singularity at the three-phase contact line and determination of the dynamic contact angle. The works of Huh & Scriven (1971) and Dussan V. & Davis (1974) highlight the fundamental difficulties associated with the dynamic contact line problem formulated in the framework of conventional fluid mechanics.

Over the years several theories and models have been proposed to remove the singularity and to provide a proper description of the fluid mechanics of moving contact lines. One of the most popular approaches has been the replacement of the no-slip boundary condition with a Navier slip model (see for example Dussan V. 1979; Hocking 1992; and Haley & Miksis 1991) while recently a theory which treats dynamic wetting as a particular case of a more general physical phenomenon, namely the process by which interfaces form or disappear within a flow, has been developed by Shikhmurzaev (1997).

The associated problem of the stability of moving contact lines has similarly received considerable attention over the years, a characteristic feature being that when the flow becomes unstable it develops fingers at the leading edge of the spreading liquid. The instability is observed under conditions of forced wetting when the contact line is driven by gravity or other body forces.

The fingering instability of a thin viscous liquid sheet of fixed volume spreading under the action of gravity on a dry inclined plane was first studied by Huppert (1982). His pioneering study showed that the initially two-dimensional liquid mass develops an instability in the transverse direction that eventually grows into well-defined fingers. Huppert's experiments as well as the more recent experiments by Silvi & Dussan V. (1985) also revealed the existence of two patterns for the fingers that

developed depending on the wettability characteristics of the solid–liquid pair. The same type of instability has been observed (Melo, Joanny & Fauve 1989; Fraysse & Homsy 1994) in the problem of a drop spinning on an horizontal substrate where the bulk force density exhibits a linear dependence on the distance from the axis of rotation – the gravitational force is now replaced with the centrifugal acceleration.

The base flow before the onset of the instability has been characterized by Troian *et al.* (1989), Hocking (1990) and Moriarty, Schwartz & Tuck (1991). Their analyses show that the front is a capillary ridge where all forces – surface tension, viscous and body force – balance. Significant progress towards the understanding of the linear stage of the instability was achieved with the works of Troian *et al.* (1989) and more recently Spaid (1995), Spaid & Homsy (1996) and Bertozzi & Brenner (1997) who performed a linear stability analysis of the capillary ridge in the transverse direction. All these works have pointed out that fingering is closely connected with the capillary hump and have revealed the existence of a preferred wavelength for the instability in the spanwise direction. Qualitative agreement with the theoretical predictions for the instability wavelength was demonstrated by Fraysse & Homsy (1994) and de Bruyn (1992).

The nonlinear stage of the fingering instability is considered in this study. The presence of a constant-thickness precursor film is assumed at the front of the contact line as has been done by Troian *et al.* (1989), Moriarty *et al.* (1991), Spaid & Homsy (1996) and Bertozzi & Brenner (1997). The precursor film model conveniently removes the stress singularity associated with the presence of a true contact line and the classical no-slip boundary condition applies everywhere on the solid substrate. The situation is then similar to that of a liquid mass flowing on a pre-wetted plane. Using methods from dynamical systems, we develop a theory for the weakly nonlinear stage of the instability. More specifically, the linearized operator of the nonlinear system yields a spectrum with a zero eigenvalue well isolated from the higher-order negative eigenvalues. Such nonlinear systems exhibit unique nonlinear dynamics near the equilibrium points: any sufficiently rich initial disturbance will excite all the modes in the spectrum; however, for small- but finite-amplitude disturbances, the modes associated with the negative eigenvalues will relax very rapidly and the system trajectory will approach exponentially fast an invariant manifold of the same dimension as the number of zero eigenvalues. Hence, instead of modelling the entire infinite-dimensional nonlinear dynamics, one needs only to decipher the low-dimensional and slow nonlinear dynamics on the invariant manifold. We shall also demonstrate that the instability is a phase instability with growth due to the translational invariance of the system in the streamwise direction. The nonlinear evolution is governed by a Kuramoto–Sivashinsky-type partial differential equation whose solution is a saw-tooth pattern for the fingers for small values of the precursor film thickness while the presence of a thick precursor prevents the instability.

2. Formulation

A thin viscous current is flowing down an inclined plane under the action of gravity (see figure 1). Assuming small slopes and creeping flow conditions, the standard lubrication approximation is (Troian *et al.* 1989; Schwartz 1989; Goodwin & Homsy 1991)

$$\frac{\partial h}{\partial t} + \nabla \left\{ h^3 \left[\boldsymbol{i} + B^{-1} \nabla \left(h_{xx} + h_{yy} \right) \right] \right\} = 0 \tag{2.1}$$

where h is the dimensionless film thickness in the z-direction (h, x and y have been non-dimensionalized with a characteristic lengthscale ℓ_c in the x-direction which

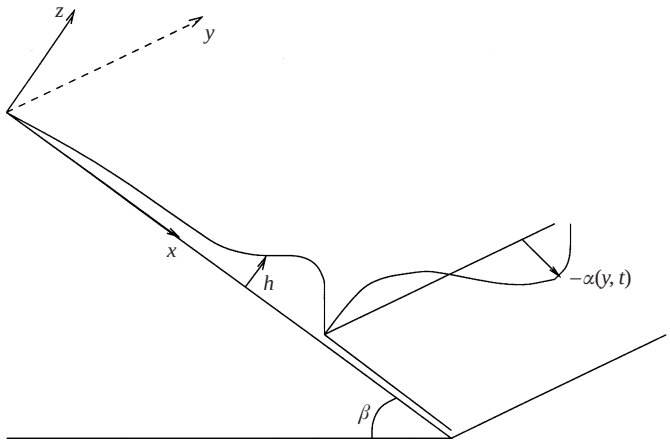

FIGURE 1. Viscous current down a slope. The location of the apparent contact line is given by $-\alpha(y,t)$.

can be defined as the length of the liquid mass in this direction at time 0), $\boldsymbol{i}$ is the unit vector in the streamwise direction and B^{-1} is an inverse Bond number defined $B = \ell_c^2 \varrho g \sin\beta/\sigma$ with ϱ and σ the density and surface tension of the liquid respectively, g the gravitational acceleration and β the angle between the inclined plane and the horizontal direction. Time in (2.1) has been non-dimensionalized with the time scale associated with viscous gravitational drainage, $3\mu/(\varrho g \sin\beta \ell_c)$ where μ is the viscosity of the liquid. Note that in (2.1) the hydrostatic head due to gravity in the direction perpendicular to the solid boundary has been neglected. According to Troian *et al.* (1989) this is indeed the case for $Ca^{1/3} \ll \tan\beta$, i.e. for the large inclination angles considered here (the capillary number is defined as $Ca = \mu U/\sigma$ with U a typical contact line speed (Troian *et al.* 1989; Hocking 1990)).

Following Troian *et al.* (1989) and Moriarty *et al.* (1991), the surface tension forces are small compared to the viscous and gravitational forces, that is $B \gg 1$ (indeed this is the case in experiments (Huppert 1982; Melo *et al.* 1989; Fraysse & Homsy 1994)), and the curvature terms in (2.1) can be neglected to leading order. The resulting nonlinear hyperbolic partial differential equation for the region where viscous and gravitational forces balance was solved by Huppert using the method of characteristics to obtain the film height

$$h_0(x,t) = 3^{-1/2} x^{1/2} t^{-1/2} \tag{2.2}$$

where $0 \leqslant x \leqslant \Gamma_0$ with $x = \Gamma_0$ the location of the unperturbed contact line

$$\Gamma_0(t) = (3/2)^{2/3} 3^{1/3} t^{1/3}. \tag{2.3}$$

The solution given by (2.2) is simply a shock that ends at $x = \Gamma_0$ with height $H_0 = 2^{-1/3} t^{-1/3}$. We can now obtain an expression for the capillary number as a function of the physical parameters in the problem: by definition $Ca = \mu U/\sigma$ where $U = \ell_c[(\rho g \sin\beta \ell_c)/3\mu] \times (\mathrm{d}\Gamma_0/\mathrm{d}t)$ such that $Ca = (1/3)B(\mathrm{d}\Gamma_0/\mathrm{d}t)$ and $Ca \ll 1$ for $t \gg B^{3/2}$ with $\mathrm{d}\Gamma_0/\mathrm{d}t = O(t^{-2/3})$ from (2.3).

In the region close to the contact line the surface tension terms are no longer negligible. These nonlinear diffusion terms must be included in a thin boundary layer in order to smooth out the discontinuity of the shock in (2.2). A number of authors (Troian *et al.* 1989; Hocking 1990; Moriarty *et al.* 1991; Fraysse & Homsy 1994)

recognized that the problem is a singular perturbation one with a small parameter multiplying the higher-order derivatives in equation (2.1). Therefore, in the region close to the contact line we introduce the inner coordinates

$$h = H_0(t)\Phi^*(v), \quad v = H_0{}^{-1/3}B^{1/3}(x - \Gamma_0) \tag{2.4}$$

where v is a coordinate moving with the speed of the unperturbed contact line, and the one-dimensional version of (2.1) can be written as

$$B^{-1/3}H_0^{-8/3}\dot{H}_0\Phi^* - \tfrac{1}{3}B^{-1/3}\dot{H}_0H_0^{-8/3}v\Phi_v^* - H_0^{-2}\dot{\Gamma}_0\Phi_v^* + (\Phi^{*3})_v + (\Phi^{*3}\Phi_{vvv}^*)_v = 0,$$

where the dot denotes differentiation with respect to time. The first two terms in the above equation are $O(B^{-1/3}t^{-4/9})$ and can be safely omitted compared with the other terms:

$$-H_0^{-2}\dot{\Gamma}_0\Phi_v^* + (\Phi^{*3})_v + (\Phi^{*3}\Phi_{vvv}^*)_v = 0. \tag{2.5}$$

Hence, the time-derivative term in (2.1) only contributes through the dependence of $H_0^{-2}\dot{\Gamma}_0$ on time and the inner region is quasi-steady to leading order (see for example Hocking 1990 and Moriarty *et al.* 1991).

At the front of the contact line we assume the presence of a constant-thickness precursor film as was first proposed by Troian *et al.* (1989), thus circumventing the difficulties associated with the presence of a true contact line (the contact line simply becomes an apparent one). The model is appropriate for wetting fluids only: we can argue that partially wetting fluids cannot sustain flat thin films without rupture and subsequent de-wetting (Veretennikov, Indeikina & Chang 1998). The situation is then similar to that of a thin liquid mass of a perfectly wetting fluid flowing on an inclined plane pre-wetted with a thin flat film of the same fluid. We also assume that the precursor film thickness is large enough so that long-range attractive intermolecular interactions between the solid and gas molecules separated by the liquid phase are not significant. These forces generate a disjoining pressure for thicknesses of the order of 1 to 100 nm (Teletzke, Davis & Scriven 1987; Schwartz & Eley 1998) and they are responsible for the formation of a front-running precursor film that exponentially decays to zero ahead of the macroscopic front of completely wetting fluids spreading on dry surfaces (de Gennes 1985; Kalliadasis & Chang 1994*a*; Kalliadasis & Chang 1996).

We can now integrate (2.5) once with respect to v and fix the integration constant by demanding that $h = H_0$ is a solution (this represents matching to the outer region $h_0(x,t)$ as $v \to -\infty$). To match to a precursor film of thickness b at the front of the contact line we note that $\dot{\Gamma}_0(H_0 - b) = H_0^3 - b^3$ from conservation of mass considerations and, with $\delta = b/H_0$, (2.5) becomes the equation for the capillary ridge that smooths out Huppert's outer solution:

$$\Phi_{vvv}^* = -\frac{\delta + \delta^2}{\Phi^{*3}} + \frac{1 + \delta + \delta^2}{\Phi^{*2}} - 1. \tag{2.6}$$

This was first derived by Troian *et al.* (1989). In a three-dimensional phase space the inner region is a heteroclinic orbit that connects the two stable fixed points $\Phi^* = 1$ and $\Phi^* = \delta$ and has to be obtained numerically with the boundary conditions $\Phi^* \to 1$ as $v \to -\infty$ and $\Phi^* \to \delta$ as $v \to +\infty$. The numerical solution of (2.6) is discussed by Tuck & Schwartz (1990). Finally, notice that time t in (2.6) plays a parametric role through the dependence of H_0 on t; however, although H_0 decreases with time, it is assumed to evolve on a slow time scale compared to the faster fingering time scale and such that the front is quasi-steady.

To analyse the nonlinear stage of the instability we note that for $B \gg 1$, the capillary ridge, which is now two-dimensional, is restricted to a region close to the contact line. This observation is consistent with the experimental data by Melo *et al.* (1989) for the spin coating problem which clearly demonstrate that even when the fingers are well developed – at least in the weakly nonlinear regime of the instability – the ridge is restricted to an area close to the contact line. Simple stability arguments presented by Hocking (1990), show that the outer region is linearly stable and the instability is closely connected with the inner domain. We then introduce in (2.1) the similarity transformation

$$h = H_0(t)\Phi(v, w, t), \quad v = H_0^{-1/3}B^{1/3}(x - \Gamma_0), \quad w = H_0^{-1/3}B^{1/3}y$$

to obtain

$$\dot{H}_0 B^{-1/3}H_0^{-8/3}\Phi - \tfrac{1}{3}\dot{H}_0 B^{-1/3}H_0^{-8/3}v\Phi_v + H_0^{-5/3}B^{-1/3}\Phi_t - \dot{\Gamma}_0 H_0^{-2}\Phi_v + (\Phi^3)_v + \frac{\partial}{\partial v}\left[\Phi^3\frac{\partial}{\partial v}(\Phi_{vv} + \Phi_{ww})\right] + \frac{\partial}{\partial w}\left[\Phi^3\frac{\partial}{\partial w}(\Phi_{vv} + \Phi_{ww})\right] = 0.$$

As with the derivation of (2.5) the first two terms in the above equation are $O(B^{-1/3}t^{-4/9})$ and can be safely neglected. The time-dependent coefficient of Φ_t can be scaled away by introducing a modified time scale τ first proposed by Troian *et al.* (1989) for the linear stability analysis of the capillary ridge: $B^{-1/3}H_0^{-5/3}\Phi_t = \Phi_\tau$ or $\tau = (9/4)2^{-5/9}B^{1/3}t^{4/9}$ to leading order in δ, and with $\dot{\Gamma}_0/H_0^2 = 1 + \delta + \delta^2$ we obtain the basic equation for the analysis to follow:

$$\Phi_\tau - (1 + \delta + \delta^2)\Phi_v + (\Phi^3)_v + \frac{\partial}{\partial v}\left[\Phi^3\frac{\partial}{\partial v}(\Phi_{vv} + \Phi_{ww})\right] + \frac{\partial}{\partial w}\left[\Phi^3\frac{\partial}{\partial w}(\Phi_{vv} + \Phi_{ww})\right] = 0. \tag{2.7}$$

We now introduce a long scale in the transverse direction $r = \epsilon w$ with $\epsilon \ll 1$. The presence of this slow scale signifies the slow variation of Φ in the w-direction at least in the weakly nonlinear stage of the instability. We also introduce a disturbance $v(v, r, \tau)$ with $\Phi(v, r, \tau) = \Phi^*(v) + v(v, r, \tau)$ which when substituted into (2.7) using (2.6) yields the disturbance equation

$$v_\tau = \mathscr{L}v + \sum_1^3 N_i(v) + \epsilon^2\sum_4^7 N_i(v) + \epsilon^4\sum_8^{11} N_i(v) \tag{2.8}$$

where the linear operator $\mathscr{L}$ is defined as

$$\mathscr{L} = -2(1 + \delta + \delta^2)\frac{\partial}{\partial v} + 3(\delta + \delta^2)\frac{\partial}{\partial v}\left[\frac{(\cdot)}{\Phi^*}\right] - \frac{\partial}{\partial v}\left[\Phi^{*3}\frac{\partial^3}{\partial v^3}(\cdot)\right] \tag{2.9}$$

and the nonlinearities N_i are given by

$$N_1(v) = -\frac{\partial}{\partial v}\left(3\Phi^* v^2 + 3\Phi^{*2}vv_{vvv} + 3\Phi^*\Phi^*_{vvv}v^2\right),$$

$$N_2(v) = -\frac{\partial}{\partial v}\left(v^3 + 3\Phi^* v^2 v_{vvv} + \Phi^*_{vvv}v^3\right), \quad N_3(v) = -\frac{\partial}{\partial v}\left(v^3 v_{vvv}\right),$$

$$N_4(v) = -\frac{\partial}{\partial v}\left(\Phi^{*3}v_{rrv}\right) - \frac{\partial}{\partial r}\left(\Phi^{*3}v_{vvr}\right),$$

$$N_5(v) = -\frac{\partial}{\partial v}\left(3\Phi^{*2}vv_{rrv}\right) - \frac{\partial}{\partial r}\left(3\Phi^{*2}vv_{vvr}\right),$$

$$N_6(v) = -\frac{\partial}{\partial v}\left(3\Phi^{*}v^2v_{rrv}\right) - \frac{\partial}{\partial r}\left(3\Phi^{*}v^2v_{vvr}\right), \quad N_7(v) = -\frac{\partial}{\partial v}\left(v^3v_{rrv}\right) - \frac{\partial}{\partial r}\left(v^3v_{vvr}\right),$$

$$N_8(v) = -\frac{\partial}{\partial r}\left(\Phi^{*3}v_{rrr}\right), \quad N_9(v) = -\frac{\partial}{\partial r}\left(3\Phi^{*2}vv_{rrr}\right),$$

$$N_{10}(v) = -\frac{\partial}{\partial r}\left(3\Phi^{*}v^2v_{rrr}\right), \quad N_{11}(v) = -\frac{\partial}{\partial r}\left(v^3v_{rrr}\right).$$

The eigenfunctions Φ_k and eigenvalues λ_k of $\mathscr{L}$ are defined from the eigenvalue problem

$$\mathscr{L}\Phi_k = \lambda_k\Phi_k, \quad \Phi_k(v \to \pm\infty) = 0, \qquad k = 0, 1, 2, \ldots . \tag{2.10}$$

The boundary conditions are decaying functions at infinity, thus restricting our attention to localized disturbances associated with the discrete spectrum of $\mathscr{L}$. The continuous spectrum will consist of those eigenfunctions with bounded oscillatory behaviour as $v \to \pm\infty$, and while we expect at least part of this continuous spectrum to be excited, since the flat films far from the capillary hump are unstable to periodic disturbances of certain wavelength, we can assume that these modes are swept away by the faster moving capillary hump and are hence unimportant to the dynamics of the front (similar assumptions have been made in stability studies of solitary waves on falling films (Chang, Demekhin & Kopelevich 1995, 1996)). Alternatively, the disturbances should not alter the base flow far from the hump and $\Phi \to 1$ as $v \to -\infty, \Phi \to \delta$ as $v \to +\infty$.

The adjoint operator $\mathscr{L}^*$ is defined with respect to the usual $L^2(-\infty, +\infty)$ inner product $\langle f, g\rangle = \int_{-\infty}^{+\infty} f\bar{g}\mathrm{d}v$ (the overbar designates complex conjugation) for any two functions f and g with appropriate boundary conditions at infinity and such that $\langle \mathscr{L}f, g\rangle = \langle f, \mathscr{L}^*g\rangle$ (we note that $\mathscr{L}$ is not self-adjoint and the discrete eigenvalues and eigenfunctions can be complex). A simple integration by parts yields

$$\mathscr{L}^* = -(1+\delta+\delta^2)\frac{\partial}{\partial v} + 3\Phi^{*2}\frac{\partial}{\partial v} + 3\Phi^{*2}\Phi^*_{vvv}\frac{\partial}{\partial v} - \frac{\partial^3}{\partial v^3}\left[\Phi^{*3}\frac{\partial}{\partial v}(\cdot)\right] \tag{2.11}$$

and the adjoint eigenvalue problem is defined from

$$\mathscr{L}^*\hat{\Phi}_k = \bar{\lambda}_k\hat{\Phi}_k, \quad \frac{\partial\hat{\Phi}_k}{\partial v}(v \to \pm\infty) = 0, \qquad k = 0, 1, 2, \ldots . \tag{2.12}$$

By differentiating now the defining equation (2.6) for the capillary ridge twice with respect to v one obtains

$$\mathscr{L}\Phi^*_v = 0, \tag{2.13a}$$

and

$$\Phi_0 = \Phi^*_v \tag{2.13b}$$

is a null eigenfunction corresponding to the eigenvalue $\lambda_0 = 0$. This eigenfunction is a key component in the present theory and it is associated with the translational invariance of the system in the v-direction: since equation (2.6) for the capillary ridge is invariant to a shift in v, if Φ^* is a solution, so must be its translate $\Phi^*(v - v_0(t))$ and hence there is a family of possible solutions generated by the translation. If one perturbs the capillary hump by translating it slightly, that is $v_0(t) \ll 1$, then

$$\Phi^*(v - v_0(t)) \sim \Phi^*(v) - v_0(t)\Phi^*_v(v) \tag{2.14}$$

where $v_0(t)\Phi^*{}_v(v)$ is the perturbation due to translation. Equation (2.14) can now be substituted into (2.6) and after linearizing for $v_0 \ll 1$ and differentiating the resulting equation once with respect to v one obtains (2.13*a*): the translational symmetry manifests itself as a null eigenfunction.

The ultimate goal of our study is the derivation of an evolution equation for the location of the fingers in the weakly nonlinear regime of the instability. We shall now derive the functional form of this equation using qualitative arguments based on simple symmetry and global constraint considerations prior to the formal derivation in the next section. For this purpose we decompose v into eigenmodes $v = \alpha\Phi_0(v) + \sum_{i=1}^{\infty} v_i\Phi_i$ (and thus by taking appropriate inner products with the adjoint eigenfunctions the disturbance equation (2.8) can be reduced to a system of partial differential equations for $\alpha(w,\tau)$ and $v_i(w,\tau)$). We now assume that all the higher-order eigenvalues of $\mathscr{L}$ lie in the left half of the complex λ-plane and at a finite distance from the imaginary axis or equivalently the higher-order modes v_i associated with these eigenvalues are stable (this assumption has been rigorously verified by a numerical solution of the eigenvalue problem in (2.10) – see the next section). As time advances to unit order the evolution of the v_i modes is much faster than that of α. This asymptotic evolution will then be 'adiabatically' coupled to α and the coupling can be simply obtained by invoking the quasi-steady approximation $\partial v_i/\partial\tau \approx 0$. Therefore, in the vicinity of the instability, we are left with only one relevant dynamical variable, the 'critical' mode $\alpha(w,\tau)$ which varies on a time scale much slower than that of the other modes and thus contains all the information about the asymptotic time dependence of v near the instability onset. The basic idea of the nonlinear analysis of the next section is to eliminate adiabatically the fast modes to obtain an evolution equation for $\alpha(w,\tau)$.

We now relate α to the perturbation of the apparent contact line boundary v_B since (2.8) is a disturbance equation for the front height only: with $\Phi = \Phi^* + v$ where $v \sim \alpha\Phi_0$ to leading order, one obtains $\Phi \sim \Phi^* + \alpha\Phi_v^*$. For $v_B, \delta \ll 1$, a Taylor series expansion of $\Phi(v_B)$ as $v \to 0^-$, which represents the location of the unperturbed contact line, shows that

$$v_B \sim -\alpha \tag{2.15}$$

where terms $O(\alpha v_B)$ have been neglected and hence the leading-order mode $\alpha(w,\tau)$ gives the negative amplitude of the fingers in the weakly nonlinear stage of the instability and in a frame of reference moving with the unperturbed contact line. We now notice that the fundamental equation (2.1) is symmetric under $y \to -y$ or $w \to -w$. We therefore expect the evolution equation to contain only even terms in w and since the system is dissipative, no time-reversal symmetry is allowed. These considerations lead to the linear evolution equation for the finger location $\alpha_\tau + \alpha_{ww} + \alpha_{wwww} = 0$ with the effects of instability and dissipation represented by the second- and fourth-order derivatives respectively (the linearized form of the evolution equation can also be obtained by a Fourier transform of the linearized form of (2.8)) and with the fourth-order derivative α_{wwww} causing damping to counterbalance the instability term α_{ww}. For the quadratic nonlinear terms we notice that the only possible nonlinearities with respect to w are α^2, α_w^2, $\alpha\alpha_{ww}$, α_{ww}^2 and $(\alpha\alpha_w)_w$. An inspection of the nonlinearities for the disturbance v in (2.8) eliminates α_w^2 and α_{ww}^2. The α^2 nonlinearity would originate from N_1 in (2.8) and the $\alpha\alpha_{ww}$ and $(\alpha\alpha_w)_w$ nonlinearities from N_5 in (2.8) respectively. The nonlinearities α^2 and $\alpha\alpha_{ww}$ do not conserve mass for periodic boundary conditions on a domain L in the transverse w-direction as a simple integration of (2.8) from $v \to -\infty$ to $v \to +\infty$ and $w = -L/2$ to $w = L/2$

reveals:

$$\int_{-\infty}^{+\infty}\int_{-L/2}^{L/2}\frac{\partial v}{\partial \tau}\mathrm{d}w\mathrm{d}\tau = 0$$

which with $v \sim \alpha\Phi_v^*$ gives

$$\frac{\partial}{\partial \tau}\int_{-L/2}^{L/2}\alpha \mathrm{d}w = 0.$$

This leaves $(\alpha\alpha_w)_w$ as the only possible quadratic nonlinearity for the α-evolution equation. Thus, we expect an evolution equation of the form

$$\alpha_\tau + \kappa_1\alpha_{ww} + \kappa_2\alpha_{wwww} + \kappa_3(\alpha\alpha_w)_w = 0 \tag{2.16}$$

where we have implicitly assumed that the higher-order nonlinear term has the 'right sign' to saturate the dynamics within the weakly nonlinear slowly varying realm for which the equation is valid. The dependence of the coefficients $\kappa_{1,2,3}$ on the physical parameters of the problem, for instance the precursor film thickness, cannot be determined by simple symmetry considerations and a more detailed analysis will be undertaken in the next section for that purpose. Nevertheless it is the symmetry $y \to -y$ and conservation of volume that determine the form of the quadratic nonlinearity.

3. Derivation of the fingering evolution equation using centre manifold projection

We now offer a rigorous derivation of (2.16) which will allow us to obtain the coefficients of the evolution equation. Our starting point is the eigenvalue problem in (2.10). The higher-order eigenfunctions of $\mathscr{L}$ must be constructed numerically. For this purpose we adopted the method of orthogonalizations suggested by Conte (1966) appropriately modified to account for the infinite domain considered here and used by Spaid (1995) and Spaid & Homsy (1996) for the solution of the eigenvalue problem governing the linear stability of the capillary hump. The method eliminates parasitic growth of undesired roots at the ends of the domain and is based on shooting from both sides of the integration interval along linearly independent trajectories until a matching point is reached somewhere in the middle where a solvability condition is applied. The solutions are examined at each step and they are orthonormalized when they exceed certain non-orthogonality criteria.

The numerical scheme confirmed that $\lambda_0 = 0$ is an eigenvalue with corresponding eigenfunction Φ_v^*. For the adjoint problem, an inspection of (2.11) and (2.12) shows that $\hat{\Phi}_0 = \text{const.}$ is a null eigenfunction. The value of the constant can be selected when the inner product $\langle \Phi_0, \hat{\Phi}_0 \rangle = (\delta - 1) \times \text{const.}$ is normalized to 1. We have confirmed numerically that $\hat{\Phi}_0 = \text{const.}$ is the only null eigenfunction of $\mathscr{L}^*$. Hence, the null space of $\mathscr{L}^*$ has the same dimension as the null space of $\mathscr{L}$, 0 is an eigenvalue of geometric and algebraic multiplicity 1 and Φ_v^* forms a complete basis for the null space of $\mathscr{L}$. This is not the case for the operator associated with the stability of solitary wave solutions of the Kuramoto–Sivashinsky equation (Chang & Demekhin 1996; Elphick *et al.* 1991): the null space of the adjoint operator is two-dimensional and the localized pulse solutions have, in addition to the translational symmetry considered here, the Galilean symmetry that generates a one-parameter family of solutions by appropriately shifting the substrate thickness and speed of the solitary pulses.

The numerical method revealed that

$$\mathrm{Re}(\lambda_i) < 0, \qquad i = 1, 2, 3, \ldots, \tag{3.1}$$

with the first non-zero eigenvalue $\lambda_1 \simeq -0.55$ for $\delta = 0.1$. For the numerical construction of the eigenfunctions we note that $\int_{-\infty}^{+\infty} \Phi_k \mathrm{d}v = 0$ for $k \neq 0$ as a simple integration of (2.10) shows. This property implies that the higher-order discrete modes do not carry mass (due to the gradient-flow form of the evolution equation (2.1) associated with mass conservation) and can be used as a means of checking the accuracy of the numerical method. The method also requires the boundary conditions for the higher-order adjoint eigenfunctions: it follows from (2.12) that $\hat{\Phi}_k (k \neq 0) \to 0$ as $v \to \pm\infty$.

We now expand the disturbance v in (2.8) as

$$v(\tau, r, v) = \alpha(\tau, r)\Phi_0(v) + \hat{v}(\tau, r, v) \tag{3.2a}$$

where $\hat{v}$ is the complement with respect to the null eigenfunction Φ_0. By introducing the operator $\mathscr{P}$ to denote projection onto the null space,

$$\mathscr{P} f = \langle f, \hat{\Phi}_0 \rangle \Phi_0, \tag{3.2b}$$

and the complementary projection operator $\mathscr{I} - \mathscr{P}$ to denote projection onto the complement of Φ_0,

$$(\mathscr{I} - \mathscr{P}) f = \sum_{i=1}^{\infty} \langle f, \hat{\Phi}_i \rangle \Phi_i \tag{3.2c}$$

for any function f in the domain of $\mathscr{L}$, the disturbance v can be written as

$$v = \mathscr{P} v + (\mathscr{I} - \mathscr{P}) v. \tag{3.2d}$$

The above expansion is a real-valued sum even when complex eigenvalues and eigenfunctions are present: indeed for real operators complex eigenvalues and eigenfunctions appear in conjugate pairs and hence if $\langle v, \hat{\Phi}_k \rangle$, $\langle v, \hat{\Phi}_{k+1} \rangle$ are the coefficients of Φ_k and Φ_{k+1} respectively with $\lambda_{k+1} = \bar{\lambda}_k$ and $\Phi_{k+1} = \overline{\Phi}_k$, one must have $\langle v, \hat{\Phi}_{k+1} \rangle = \int_{-\infty}^{+\infty} v \overline{\hat{\Phi}}_{k+1} \, \mathrm{d}v = \langle \hat{\Phi}_k, v \rangle = \overline{\langle v, \hat{\Phi}_k \rangle}$.

Substituting (3.2*d*) into (2.8), taking inner products of both sides of the resulting equation with $\hat{\Phi}_0$, $\hat{\Phi}_i (i \neq 0)$ and using the orthonormalization relation $\langle \Phi_i, \hat{\Phi}_j \rangle = \delta_{ij}$ gives the equations

$$\alpha_\tau = \left\langle \sum_1^3 N_i(\alpha\Phi_0 + \hat{v}), \hat{\Phi}_0 \right\rangle + \epsilon^2 \left\langle \sum_4^7 N_i(\alpha\Phi_0 + \hat{v}), \hat{\Phi}_0 \right\rangle + \epsilon^4 \left\langle \sum_8^{11} N_i(\alpha\Phi_0 + \hat{v}), \hat{\Phi}_0 \right\rangle \tag{3.3a}$$

and

$$\hat{v}_\tau = \mathscr{L}\hat{v} + (\mathscr{I} - \mathscr{P}) \sum_1^3 N_i(\alpha\Phi_0 + \hat{v}) + \epsilon^2 (\mathscr{I} - \mathscr{P}) \sum_4^7 N_i(\alpha\Phi_0 + \hat{v}) + \epsilon^4 (\mathscr{I} - \mathscr{P}) \sum_8^{11} N_i(\alpha\Phi_0 + \hat{v}). \tag{3.3b}$$

The first step of our weakly nonlinear analysis involves writing equations (3.3 *a*, *b*) in the following extended manner:

$$\alpha_\tau = F(\hat{v}, \alpha), \tag{3.4a}$$

$$\hat{v}_\tau = \mathscr{L}\hat{v} + G(\hat{v}, \alpha), \tag{3.4b}$$

$$(\epsilon^2)_\tau = 0, \tag{3.4c}$$

where the nonlinear functions F and G are given in (3.3 *a*, *b*) and ϵ^2 is now our small parameter. Recall that the real part of all eigenvalues of $\mathscr{L}$ is negative and the zero eigenvalue is well isolated. The centre manifold theorem (Carr 1981; Guckenheimer & Holmes 1983; Roberts 1988; Chang 1989; Cheng & Chang 1990; Fujimura 1991) then states that the system (3.4 *a-c*) has a two-dimensional centre manifold given by the adiabatic coupling $\hat{v} = \hat{v}(\alpha, \epsilon^2) = O(2)$ to leading order with respect to α, ϵ^2. Not only does the centre manifold theorem stipulate the existence of the centre manifold, it also ensures that this manifold is attracting at large times. To obtain the flow onto the centre manifold we note that $\alpha_\tau = O(2)$ so that $\hat{v}_\tau = O(3)$ and the leading-order centre manifold projection (tangent-space approximation) is simply

$$\hat{v}_\tau \sim 0 \tag{3.5a}$$

or

$$\mathscr{L}\hat{v} \sim \alpha^2(\mathscr{I} - \mathscr{P})\frac{\partial}{\partial v}\left[(3\Phi^* + 3\Phi^*\Phi^*_{vvv})\Phi_0^2 + 3\Phi^{*2}\Phi_0\Phi_{0vvv}\right] + \epsilon^2\alpha_{rr}(\mathscr{I} - \mathscr{P})\left[\frac{\partial}{\partial v}(\Phi^{*3}\Phi_{0v}) + \Phi^{*3}\Phi_{0vv}\right] + O(3). \tag{3.5b}$$

Note that $\mathscr{L}$ is a singular operator and the right-hand side of (3.5*b*) must satisfy the Fredholm alternative solvability condition $\langle \mathrm{RHS}, \hat{\Phi}_0 \rangle = 0$; it does so since the null eigenfunction has been removed via the complementary projection operator $\mathscr{I} - \mathscr{P}$.

Inverting $\mathscr{L}$ in (3.5*b*) yields the leading-order centre manifold projection

$$\hat{v} \sim \alpha^2 f_2(v) + \epsilon^2\alpha_{rr} f_3(v) + O(3) \tag{3.6}$$

where

$$f_2(v) = \sum_{i=1}^{\infty} \frac{1}{\lambda_i}\langle f_0, \hat{\Phi}_i\rangle \Phi_i, \qquad f_3(v) = \sum_{i=1}^{\infty} \frac{1}{\lambda_i}\langle f_1, \hat{\Phi}_i\rangle \Phi_i$$

with

$$f_0(v) = \frac{\partial}{\partial v}[(3\Phi^* + 3\Phi^*\Phi^*_{vvv})\Phi_0^2 + 3\Phi^{*2}\Phi_0\Phi_{0vvv}]$$

and

$$f_1(v) = \frac{\partial}{\partial v}(\Phi^{*3}\Phi_{0v} + \Phi^{*3}\Phi_{0vv}).$$

The series in $f_2(v)$ and $f_3(v)$ converge fast by using the first few eigenvalues and eigenfunctions (it was found that the number of eigenfunctions necessary for convergence increased with decreasing δ). Higher-order corrections to the leading-order centre manifold projection (3.6) can be obtained with standard techniques based on Taylor series expansion of $\hat{v}$ at the origin (Carr 1981; Guckenheimer & Holmes 1983).

The dynamics on the centre manifold is governed by the slow equation (3.3*a*) with $\hat{v}$ given by (3.6). We note that $\hat{v}$ in (3.3*a*) appears in second- or higher-order nonlinearities and hence the approximation for α in (3.3*a*) is valid up to $O(3)$ and

terms $O(4)$ and higher must be neglected. Substituting now (3.6) into (3.3*a*) yields a nonlinear partial differential equation for the evolution of α in time and space,

$$\alpha_\tau + \chi\alpha_{ww} + \psi\alpha_{wwww} + \omega(\alpha\alpha_w)_w = 0, \tag{3.7}$$

where ϵ has now been reabsorbed in w and

$$\chi = \frac{1}{1-\delta}\langle \Phi^{*3} - (1+\delta+\delta^2)\Phi^* + \delta + \delta^2\rangle,$$

$$\psi = \frac{1}{1-\delta}(\tfrac{1}{4}(1-\delta^4) - \langle \Phi^{*3} f_{3vv}\rangle)$$

$$\omega = -\frac{1}{1-\delta}(3\langle \Phi^{*2}\Phi^*_v\Phi^*_{vvv}\rangle + 2\langle \Phi^{*3} f_{2vv}\rangle).$$

Two terms analogous to α^2 and α^3 in (3.7) are not shown since their corresponding coefficients

$$\frac{1}{1-\delta}\langle -[(3\Phi^{*2} + 3\Phi^*\Phi^*_{vvv})\Phi_0^2]_v - 3(\Phi^{*2}\Phi_0\Phi_{0vvv})_v\rangle$$

and

$$\frac{1}{1-\delta}\langle -2[(3\Phi^* + 3\Phi^*\Phi^*_{vvv})\Phi_0 f_2]_v - (\Phi_0 f_{2vvv})_v - (\Phi_{0vvv} f_2)_v\rangle$$
$$+\langle -(\Phi_0^3 + 3\Phi^*\Phi_0^2\Phi_{0vvv} + \Phi^*_{vvv}\Phi_0^3)_v\rangle$$

vanish as can be easily shown using the boundary conditions in (2.10). Note that the coefficients in (3.7) are functions of the precursor film thickness δ only with $\chi, \psi, \omega > 0$ for all δ.

All of the above analysis relies on smooth expansions in slow spatial gradients (in the transverse direction) compared with the characteristic length scales of the unperturbed front. The small parameter ϵ deserves special attention. It is associated with the introduction of a long scale in the transverse direction which approximates a 'hard' problem by writing it as a perturbation of an easier problem. We thus utilize the equation $(\epsilon^2)_\tau = 0$ to introduce the approximation of a large-scale slowly varying spatial dependence. Adjoining this equation to (3.4*a*) and (3.4*b*) focuses the subsequent centre manifold analysis upon the small-wavenumber, large-scale dynamics. Upon inspecting the details of the algebra it is apparent that ϵ just acts as a place holder for the spatial derivative $\partial/\partial w$. The adjoining of the trivial equation $(\epsilon^2)_\tau = 0$ just focuses attention upon small wavenumbers. Precisely the same effect is achieved in physical variables simply by treating $\partial/\partial w$ as 'small'. A rationale for doing this is based upon the local dynamics in any part of the domain but it is not rigorous because the operator ∂_w is unbounded and the extant theory by Gallay (1993) cannot be applied directly. Nevertheless, extensions of centre manifold analysis to very high order for other problems (see for instance Mercer & Roberts 1990) shows that the long-wave approximation actually converges for wavenumbers of $O(1)$. In this study we have restricted our attention to the leading-order centre manifold projection with the understanding that the limits to the resolution of the slowly varying, long-wave model can only be improved by retaining more dynamic modes in the model. In any case, one can approximate the shape of the centre manifold and its evolution to any order. Moreover, competing small effects may appear at any order in the analysis, they need not just arise at leading order. The centre manifold approach enables a rational

treatment of many and varied small effects, and allows any consistent truncation when the model is applied.

4. Evolution towards fingers

Several comments are now appropriate regarding equation (3.7): it is a Kuramoto–Sivashinsky-type partial differential equation for the evolution of the disturbances as the front moves down the inclined plane. The Kuramoto–Sivashinsky equation appears in several contexts–chemical oscillations, chemically reacting fronts and flames (Kuramoto 1984), falling films (Shkadov 1973; Lin 1974; Nepomnyaschy 1974; Chang 1994; Kalliadasis & Chang 1994*b*; Chang & Demekhin 1996 – see also Homsy 1974 for the generalization of this equation to include dispersion) etc. – and in that respect the nonlinear stage of the fingering instability is similar to the problem of the dynamics of slowly varying wave fronts (solitary or shock waves) arising in flame or reaction propagation (Kuramoto 1984). However, the convective term $\alpha\alpha_w$ of the Kuramoto–Sivashinsky equation is differentiated once more with respect to the spatial variable w. Physically this means that disturbances can only grow or decay without any lateral displacement due to the nonlinear kinematic effect embodied by the convective term $\alpha\alpha_w$.

Equation (3.7) can also be considered as a nonlinear diffusion equation for the diffusivity χ. Hence, the front will be unstable if and only if $\chi > 0$ as is the case here. More precisely, substituting the usual normal mode expansion $\alpha \propto \exp(\lambda\tau + \mathrm{i}kw)$ into the linearized version of (3.7), one obtains the dispersion relation

$$\lambda = \chi k^2 - \psi k^4 \tag{4.1}$$

for the growth rate λ as a function of wavenumber k. Thus small-amplitude sinusoidal disturbances are linearly unstable (growing) for long wavelengths – with a band of unstable wavenumbers that extends to zero – and stable (damping) for short wavelengths with a cut-off wavenumber $k_c = \sqrt{\chi/\psi}$. The growth rate is real and the disturbances will only grow or decay as has been already pointed out. The maximum growth rate occurs at wavenumber

$$k_m = \sqrt{\frac{\chi}{2\psi}} \tag{4.2a}$$

with wavelength

$$L_m = 2\pi\sqrt{\frac{2\psi}{\chi}}. \tag{4.2b}$$

Obviously long-wave disturbances with $k \to 0$ are always unstable and therefore the instability is a long-wave variety. In fact, it is a phase instability with growth due to translation and v_B – being the slowly varying 'phase' – is a mode with a vanishing growth rate in the long-wavelength limit: the travelling wave front $\Phi^*(v) = \Phi^*(H_0^{-1/3}B^{1/3}(x - \Gamma_0))$ is in some sense analogous to a limit-cycle solution $\mathscr{X}(t)$ of an autonomous ordinary differential equation $\mathrm{d}\mathscr{X}/\mathrm{d}t = \mathscr{F}(\mathscr{X})$, $\mathscr{X}(t+T) = \mathscr{X}(t)$ with T the period of oscillation. In fact, both have 'phase' in the sense that the translations $t \to t + t_0$ and $v \to v + v_0$ with arbitrary t_0, v_0 again yield steady solutions $\mathscr{X}(t + t_0)$, $\Phi^*(v + v_0)$ respectively. This essentially says that there always exists a zero eigenvalue (corresponding to translational disturbances) in the linearized system about $\mathscr{X}(t)$ or $\Phi^*(v)$. The analogy may persist when some weak coupling is introduced between such

modes of motion. It is quite evident what is meant by interactions between oscillators. For our travelling pulse weak coupling means that one-dimensional fronts are aligned to form a two-dimensional pulse whose front deviates slightly from a straight line and shows a slow undulatory spatial variation because the terms associated with the transverse variation are small perturbations due to the slow w-dependence of Φ.

Phase instability occurs in a large variety of hydrodynamic and reaction-diffusion systems (Kuramoto 1984; Fauve 1987) with finite-amplitude patterns subjected to long streamwise modulations or disturbances in the transverse direction. Typically a Ginzburg–Landau-type equation for the nonlinear evolution of disturbances from a large-amplitude pattern is derived using multiple-scale methods (Kuramoto 1984). The analysis presented here, based on techniques from dynamical systems theory to derive the evolution equation for the fingers (3.7), has shown that fingering from a straight front is also a phase instability.

Let us now consider the coefficients of the evolution equation (3.7) in detail by isolating the terms of (2.8) responsible for χ, ψ, ω and exploring the influence of the physical forces on these coefficients. We first notice that the term in (3.7) responsible for the onset of fingering is χa_{ww} where $\chi = \langle \Phi^{*3} \Phi_{0vv} \rangle / (\delta - 1)$ using (2.6), in agreement with the perturbation analysis by Troian *et al.* (1989) of the linear growth rate as $k \to 0$. From (2.1), the flow in the y-direction due to the x-curvature is $(\partial/\partial y)[h^3(\partial/\partial y)(h_{xx})]$ or in terms of the modified v, w variables $(\partial/\partial w)(\Phi^3 \Phi_{vvw})$ which with $\Phi \sim \Phi^* + v = \Phi^* + \alpha\Phi_0 + \hat{v}$ with $\hat{v} = O(2)$ gives to leading order $(\partial/\partial w)(\Phi^{*3} \alpha_w \Phi_{0vv}) + O(2) \sim \alpha_{ww} \Phi^{*3} \Phi_{0vv}$. Therefore, the instability is similar to the Rayleigh instability of a liquid cylinder, at least at small wavenumbers, and the response of the base flow to the leading-order disturbance $\alpha\Phi_0$ is lateral flow due to variation of the v-curvature $\alpha\Phi_{0vv}$ in the transverse direction. This is consistent with a full numerical solution of (2.1) as an initial value problem by Schwartz (1989) who observed that for $B^{-1} = 0$, i.e. in the limit of zero surface tension, fingering does not occur. For $B^{-1} \neq 0$ his numerical experiments revealed that disturbances decay initially until the curvature becomes sufficiently large at the front. At that moment lateral flow, caused by greater curvature and hence higher pressure resulting from surface tension, leads eventually to steady growth of well-defined fingers. This curvature is provided by the hump and one expects a bumpless profile to be stable. Such flat profiles have been constructed by Bertozzi & Brenner (1997) for small inclination angles where the hydrostatic head associated with the gravitational component normal to the substrate becomes important.

Using equation (2.6) for the base state we can rewrite χ as

$$\chi = \frac{1}{1-\delta} \int_{-\infty}^{\infty} (\Phi^* - 1)(\Phi^* - \delta)(\Phi^* + 1 + \delta) \mathrm{d}v,$$

first derived by Bertozzi & Brenner (1997) and valid for all inclination angles. The significance of this expression for the leading-order spectral perturbation expansion for the growth rate λ is that χ becomes negative for a bumpless profile with $\Phi^* < 1$. In this case, computation of the growth rate for all wavenumbers by Bertozzi & Brenner shows that the front is linearly stable. We can therefore adopt

$$\chi > 0$$

as a sufficient and necessary condition for instability and subsequent finger growth.

Figure 2 shows the variation of χ and maximum curvature in the streamwise direction $(\Phi^*_{vv})_{\max}$ for various δ values. This maximum curvature appears just before the dimple that links the front to the precursor film thickness. This large curvature

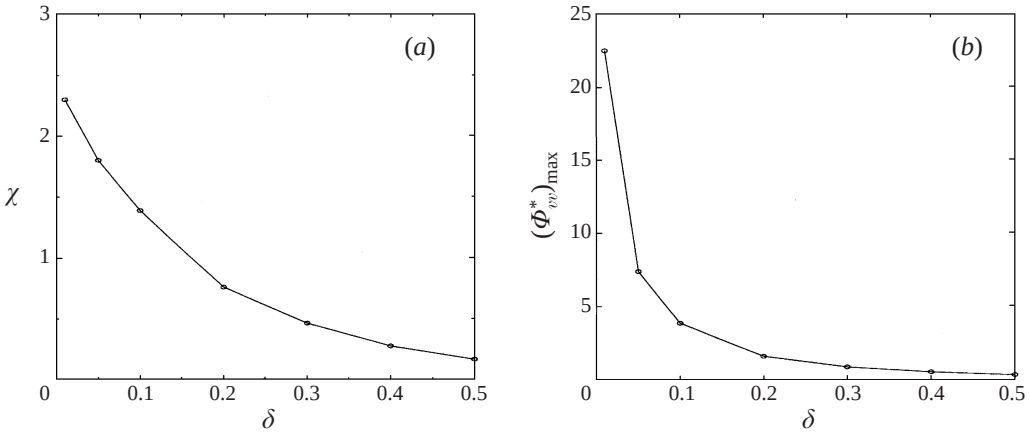

FIGURE 2. (*a*) Variation of the diffusivity χ in (3.7) with δ. The front becomes increasingly unstable for small values of the precursor film thickness. (*b*) Variation of the maximum curvature Φ^*_{vv} with δ. The v-curvature induces flow in the transverse direction leading to steady growth of fingers.

will cause high pressure resulting from surface tension and therefore flow in the transverse direction leading eventually to steady growth of fingers. As is evident from the figure both χ and $(\Phi^*_{vv})_{\max}$ decrease as δ increases and they approach zero as $\delta \to 1$ consistent with the Rayleigh instability of a liquid cylinder: the larger the radius of curvature – corresponding to smaller $(\Phi^*_{vv})_{\max}$ in our case – the more stable the cylinder.

The other two coefficients of (3.7) deserve special attention also. Consider first the coefficient ψ of the fourth-order derivative. It can be written as

$$\psi = \psi_1 + \psi_2 \tag{4.3}$$

where

$$\psi_1 = \frac{1}{1-\delta}\langle -\Phi^{*3}\Phi_0, \hat{\Phi}_0\rangle = \frac{1}{4}\frac{1-\delta^4}{1-\delta},$$

$$\psi_2 = -\frac{1}{1-\delta}\langle \Phi^{*3} f_{3vv}\rangle.$$

The ψ_1 contribution corresponds to flow in the w-direction due to variation of the w-curvature $\alpha_{ww}\Phi_0$ in that direction: indeed the flow in the y-direction due to the y-curvature (stabilizing Rayleigh term for a liquid cylinder) is $(\partial/\partial y)\left[h^3(\partial/\partial y)(h_{yy})\right]$ or in terms of the modified v, w variables $(\partial/\partial w)(\Phi^3\Phi_{www})$ which with $\Phi \sim \Phi^* + \alpha\Phi_0 + \hat{v}$ gives to leading order $(\partial/\partial w)(\Phi^{*3}\Phi^*_v\alpha_{www}) = \alpha_{wwww}\Phi^{*3}\Phi^*_v$. This contribution to ψ is always positive and acts so as to stabilize the destabilizing $\chi\alpha_{ww}$ term. Notice that ψ_1 increases for large δ as the ridge gradually decays leading to an increasingly stable front.

The ψ_2 contribution to ψ originates from the $\epsilon^2\alpha_{rr}f_3(v)$ term of $\hat{v}$ in $\epsilon^2(\partial/\partial r)(\Phi^{*3}\hat{v}_{vvr})$ of $N_4(\alpha\Phi_0 + \hat{v})$ in equation (3.3*a*), with $\hat{v} \sim \alpha^2 f_2(v) + \epsilon^2\alpha_{rr}f_3(v)$ the first higher-order correction to the leading-order disturbance $v \sim \alpha\Phi_0$. Therefore, while variation of the v-curvature of the leading-order disturbance $\alpha\Phi_0$ in the w-direction is destabilizing, variation of the v-curvature of the $\epsilon^2\alpha_{rr}f_3(v)$ higher-order term in the disturbance – as determined by centre manifold projection – is stabilizing! Our computations show

that this flow contributes mostly to the ψ_2 term and always dominates the Rayleigh term ψ_1.

Other terms may also contribute indirectly to ψ_2. For instance the flow in the v-direction due to the w-curvature

$$\frac{\partial}{\partial v}\left[\Phi^3\frac{\partial}{\partial v}(\Phi_{ww})\right] \sim \frac{\partial}{\partial v}(\Phi^{*3}\alpha_{ww}\Phi_{0v}) = \alpha_{ww}\frac{\partial}{\partial v}(\Phi^*\Phi_{0v}).$$

The contribution of this term to ψ is indirect via the $f_1(v)$ function in $f_3(v)$ which in turn is a complicated function of the eigenvalues, eigenfunctions and adjoint eigenfunctions of $\mathscr{L}$.

Consider now the coefficient ω of the only nonlinearity in the α-equation. It can be written as

$$\omega = \omega_1 + \omega_2 \tag{4.4}$$

where

$$\omega_1 = -\frac{3}{1-\delta}\langle\Phi^{*2}\Phi_v^*\Phi_{vvv}^*\rangle = 3\frac{\delta+\delta^2}{1-\delta}\ln\delta + 2(1+\delta+\delta^2)$$

and

$$\omega_2 = -\frac{2}{1-\delta}\langle\Phi^{*3}f_{2vv}\rangle.$$

Next observe that the term $(\partial/\partial y)\left[h^3(\partial/\partial y)(h_{xx}+h_{yy})\right]$ of (2.1) is responsible for the ω_1 contribution: with respect to the modified variables v, w this term can be written as

$$\begin{aligned}\frac{\partial}{\partial w}\left[\Phi^3\frac{\partial}{\partial w}(\Phi_{vv}+\Phi_{ww})\right] &= \epsilon^2\frac{\partial}{\partial r}\left[\Phi^3\frac{\partial}{\partial r}(\Phi_{vv}+\epsilon^2\Phi_{rr})\right]\\ &= \epsilon^2\frac{\partial}{\partial r}\left[(\Phi^*+v)^3\frac{\partial}{\partial r}(v_{vv}+\epsilon^2 v_{rr})\right] \sim \epsilon^2\frac{\partial}{\partial r}(\Phi^{*3}v_{vvr}+\epsilon^2\Phi^{*3}v_{rrr}+3\Phi^{*2}vv_{vvr}),\end{aligned}$$

where terms of $O(4)$ and higher have been neglected. The first two terms in the above expression correspond to the χ and ψ_1 coefficients respectively. The nonlinearity $3\Phi^{*2}vv_{vvr}$ is a 'nonlinear Rayleigh term' corresponding to the ω_1-coefficient, which may be therefore associated with the first nonlinear correction to the linear destabilizing term $\Phi^{*3}v_{vvr}$. The ω_2 contribution to ω originates from the $\alpha^2 f_2(v)$ term of $\epsilon^2(\partial/\partial r)(\Phi^{*3}\hat{v}_{vvr})$ in N_4 and can be therefore associated with the variation in the w-direction of the v-curvature of the nonlinearity $\alpha^2 f_2(v)$ in the disturbance v – as determined via centre manifold projection. The function $f_2(v)$ in turn depends on $f_0(v)$ which is composed of $(\partial/\partial v)(3\Phi^*\Phi_0^2)$ originating from $(\partial/\partial v)(3\Phi^*v^2)$, the flow in the v-direction due to the body force, and $(\partial/\partial v)(3\Phi^*vv_{vvv}+3\Phi^*v^2\Phi_{vvv}^*)$ the first nonlinear correction responsible for flow in the v-direction due to the v-curvature:

$$\begin{aligned}&\frac{\partial}{\partial v}\left[(\Phi^*+v)^3\frac{\partial}{\partial v}(\Phi_{vv}^*+v_{vv})\right]\\ &\quad= \frac{\partial}{\partial v}\left[\Phi^{*3}\Phi_{vvv}^*+\Phi^{*3}v_{vvv}+3\Phi^{*2}v\Phi_{vvv}^*+3\Phi^{*2}vv_{vvv}+3\Phi^*v^2\Phi_{vvv}^*+O(3)\right].\end{aligned}$$

Hence, it is the streamwise curvature and the body force that are responsible for the nonlinearity $(\alpha\alpha_w)_w$. Nevertheless, the front is driven by viscous, surface tension and gravity forces all coupled nonlinearly through our fundamental equation (2.1) and the above comments only provide a descriptive interpretation of the intricate combination of the various forces responsible for this unique hydrodynamic instability.

Figure 3 depicts the variation of the coefficients ψ, ω with respect to the precursor

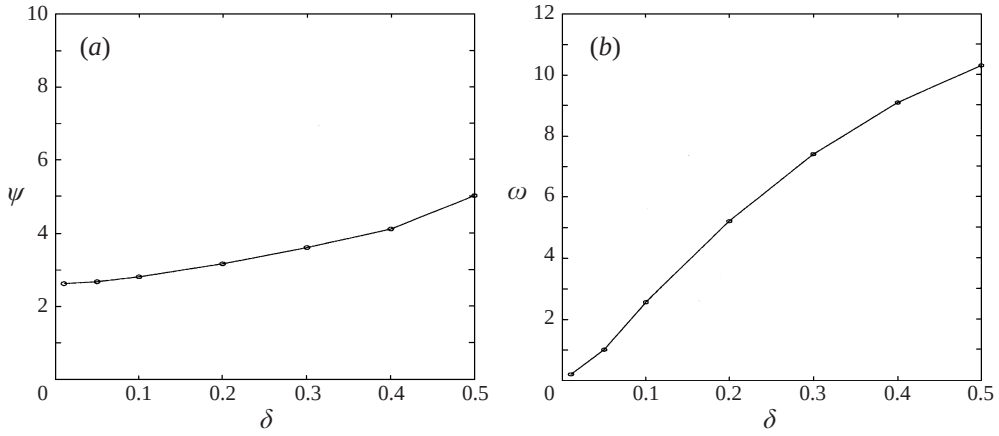

FIGURE 3. (*a*) Variation of the coefficient ψ of the fourth-order derivative in (3.7) with δ. (*b*) Variation of the coefficient ω of the nonlinearity in (3.7) with δ.

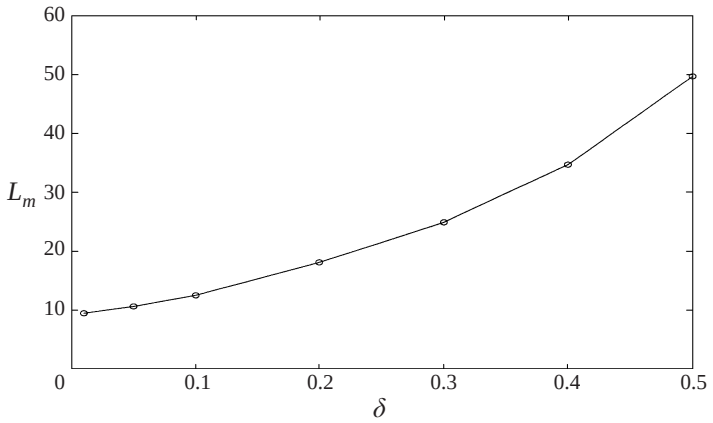

FIGURE 4. Maximum growing wavelength L_m as a function of δ.

film thickness δ. Figure 4 shows the maximum growing wavelength L_m as a function of δ. The linear stability analysis performed by a number of authors (Troian *et al.* 1989; Spaid & Homsy 1996; Bertozzi & Brenner 1997) has shown that for small δ, L_m is a weak function of δ. Figure 4 confirms this weak δ dependence with L_m varying from 12.57 at $\delta = 0.1$ to 9.50 at $\delta = 0.01$. These values are in good agreement with the value $L_m \approx 12$ reported for instance by Spaid & Homsy corresponding to a maximum growing wavenumber ≈ 0.5 for δ in the region 0.1–0.01 even though our perturbation theory is not valid at very small δ. Indeed, the eigenvalues of $\mathscr{L}$ in (2.10) can be extended away from wavenumber $k = 0$ to form different branches of the dispersion curve with (4.1) being the dominant mode (the 'phase-like' branch according to Kuramoto's terminology). The characteristic time and space scales τ_c and w_c for the instability can be estimated on the assumption that the effect of instability, represented by the $\chi\alpha_{ww}$ term in (3.7), and that of the damping $\psi\alpha_{wwww}$ and also the term α_τ are comparable in magnitude:

$$\frac{\chi}{{w_c}^2} \sim \frac{\psi}{{w_c}^4} \sim \frac{1}{\tau_c}$$

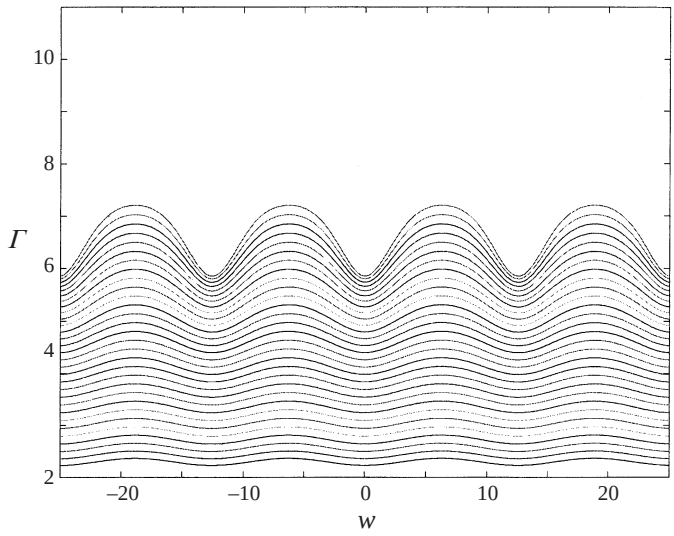

FIGURE 5. Evolution of the contact line $\Gamma(w,\tau) = \Gamma_0(\tau) + B^{-1/3}\, H_0(\tau)^{1/3}\, v_B(w,\tau)$ for $\delta = 0.1$ and $B = 10$ using the initial condition $\alpha(w,0) = 0.1\cos(2\pi w/L_m)$ in the interval $4L_m$. The lines are separated by a time interval $\Delta\tau = 0.1$.

or

$$w_c \sim \left(\frac{\psi}{\chi}\right)^{1/2}, \quad \tau_c \sim \frac{\psi}{\chi^2}.$$

The unstable fluctuations associated with the phase-like branch (4.1) are characterized by a long time scale τ_c and long space scale w_c provided that ψ is larger than χ, χ^2 which is indeed the case for large values of the precursor film thickness (see figures 2, 3). In this case the characteristic time scales of the stable fluctuations associated with the eigenvalue λ_1 in (2.10) and of unstable phase fluctuations associated with λ_0 are clearly separated. The λ_1 amplitude-like fluctuations have far shorter time scales and are expected to follow adiabatically the slow motion of the unstable phase-like fluctuations. In contrast, when the unstable phase-like fluctuations have time scales comparable to those of some amplitude fluctuations, the phase description employed here cannot completely describe the system and amplitude variation must be taken into account leading to coupled amplitude and phase equations which are beyond the scope of this study.

We shall now focus on the solutions of (3.7). Although our approach is weakly nonlinear and hence restricted to small-amplitude disturbances, it is expected that (3.7) will capture the qualitative features of the fingers' shape in the strongly nonlinear regime where the perturbation theory is no longer valid. A numerical study of the equation was carried out using an implicit Crank–Nicholson finite differencing scheme coupled with a Newton iteration for the solution of the resulting nonlinear system. We impose periodic boundary conditions on α (and therefore Φ) over a finite domain L larger than $L(k_c)$. The space and time steps are smaller than 0.1 to ensure numerical stability which is checked by examining the constancy of $\int_{-L/2}^{L/2} \alpha(w,\tau)\mathrm{d}w$ in time guaranteed from (3.7) for periodic boundary conditions.

Figure 5 depicts the temporal evolution of the contact line $\Gamma = \Gamma_0 + B^{-1/3} H_0{}^{1/3} v_B$ as a function of the modified time scale τ for $\delta = 0.1$, using the single-harmonic initial condition $\alpha(w,0) = 0.1\cos(2\pi w/L_m)$ corresponding to the maximum growing

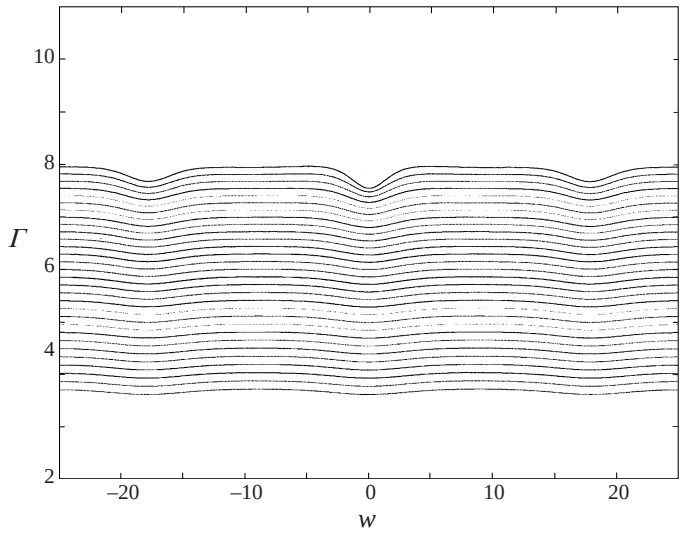

FIGURE 6. Snapshots of the contact line $\Gamma(w,\tau)$ for $\delta = 0.2$ and $B = 10$ using as initial condition a single harmonic corresponding to the maximum growing wavenumber in the interval $2.78L_m$.

wavenumber in order to speed up the evolution at small times. The values of the coefficients in (3.7) are $\chi = 1.41$, $\psi = 2.81$ and $\omega = 2.57$ with $L_m = 12.57$ and $L = 4L_m$. The inception region spans a time-scale of order $-\log(\alpha_0)/\lambda(k_m)$ with α_0 the initial amplitude. The final evolution is a series of four equally spaced fingers with the same width, speed and shape. In figure 5 we only show the last 30 snapshots of the evolution before finite-time blow-up behaviour for the zero and all higher-order derivatives of α occurred. Unlike the Kuramoto–Sivashinsky equation whose solution remains bounded for periodic boundary conditions and sufficiently smooth initial data (Kalliadasis & Chang 1994*b*), equation (3.7) exhibits blow-up behaviour for a large set of initial conditions. This unbounded growth can be arrested when higher-order nonlinearities are included in (3.7). Note that one of the most important features of the instability, the presence of an onset time as was shown experimentally by Fraysse & Homsy (1994), cannot be captured by our analysis which is asymptotically valid for large times and such that the capillary ridge in Huppert's self-similar behaviour becomes immediately unstable once formed. We therefore set arbitrarily in all our numerical integrations the 'onset time' at $t = 1$ corresponding to $\tau = 0$.

Figure 6 depicts the temporal evolution of the contact line for $\delta = 0.2$ using again a single-harmonic initial condition. The values of the coefficients in (3.7) are now $\chi = 0.76$, $\psi = 3.16$ and $\omega = 5.2$. The maximum growing wavelength is $L_m = 18.1$ almost 1.5 times larger than $L_m(\delta = 0.1)$. It is the larger value of ω in (3.7) that is responsible for the flat finger tips in figure 6 and large finger lengths in figure 5 (defined as the distance between the tip and trough). The nonlinearity in (3.7) may be identified as a nonlinear surface tension appropriately modified by the effect of the body force. For small values of the precursor film thickness δ (corresponding to small values of ω) the large capillary pressure associated with a large curvature (see figure 2) and therefore a very steep front resists fluid motion in the transverse direction. Hence, the front will break into well-defined fingers whose length will gradually increase as more liquid is supplied by the body force from the minima between subsequent fingers and therefore the troughs will gradually slow down. Notice also that as δ increases, χ

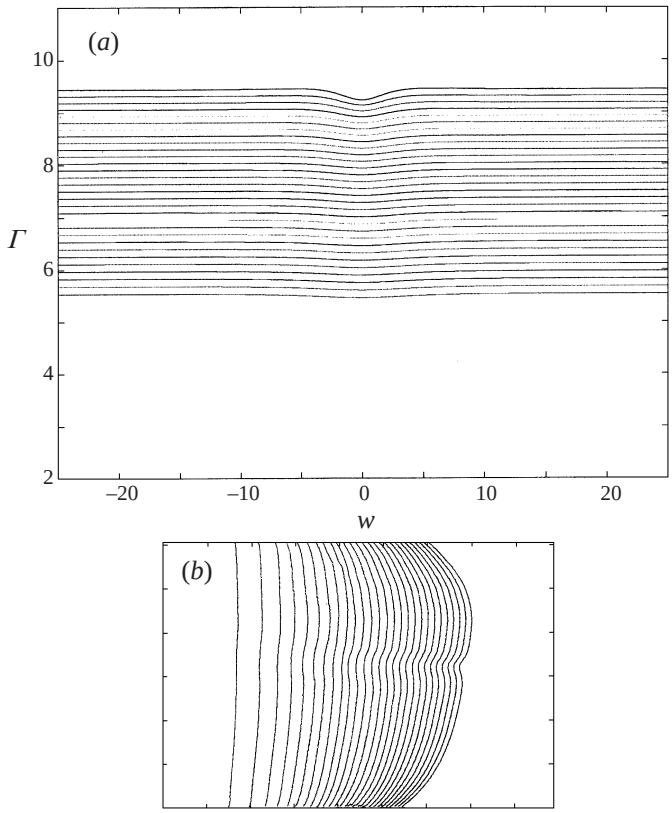

FIGURE 7. (*a*) Contact line evolution for $\delta = 0.4$ and $B = 10$ using as initial condition a single harmonic corresponding to the maximum growing wavenumber in the interval $1.45L_m$. (*b*) Fingering for Castor oil on a plane with an 8° inclination angle covered with a prewetting film (Veretennikov *et al.* 1998). Images are taken after the film has drained for 2 hours.

decreases and ψ increases (see figures 2, 3) resulting in a more stable capillary ridge. Consequently, increasing δ corresponds to decreasing the growth rate and increasing the most amplified wavelength (see figures 5, 6, 7*a*) since the maximum height and slope of the capillary ridge decrease (the ridge eventually disappears as $\delta \to 1$) and the front becomes less prone to the fingering instability.

In fact as is evident from figures 6 and 7 the presence of a thick film suppresses the instability. This seems to be consistent with the experimental finding by Melo *et al.* (1989) for the spinning drop problem that the instability is suppressed when the solid surface is pre-wetted with a thick enough film of the same liquid. However, Melo *et al.* do not report the shape of the fingers observed experimentally and clearly more experiments are needed in that direction. We also note that the number of fingers decreases when the substrate has been pre-wetted with a thick film in agreement with recent experimental data reported by Veretennikov *et al.* (1998) for small inclination angles. An interesting result concerning the precursor film model is that large δ values *do not* correspond to wetting fluids: existing experimental data with dry surfaces (Huppert 1982; Silvi & Dussan V. 1991) clearly demonstrate that completely wetting fluids develop a larger number of fingers than partially wetting ones.

Several numerical experiments with different δ values were performed. The parallel-sided fingers found experimentally for partially wetting fluids (Huppert 1982; Silvi &

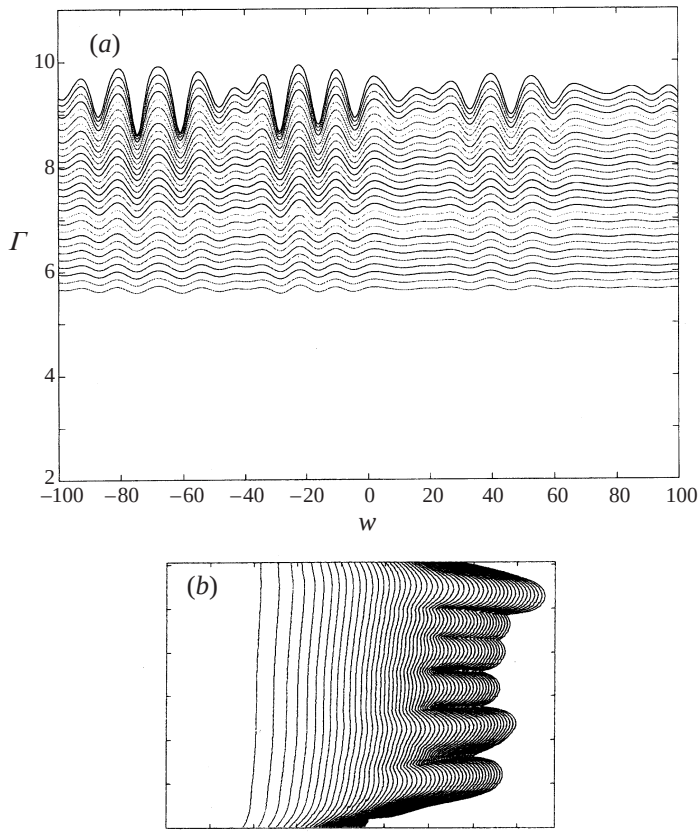

FIGURE 8. (*a*) Contact line evolution with random initial condition in the domain $16L_m$ for $\delta = 0.1$ and $B = 10$. (*b*) Fingering for Castor oil on a plane with an 8° inclination angle covered with a prewetting film (Veretennikov *et al.* 1998). Drainage now takes place for 12 hours.

Dussan V. 1991) on dry surfaces were never observed in our numerical integrations even at very small δ. In all cases the same saw-tooth pattern emerged with sharper minima at smaller δ values. The pattern seems to be qualitatively similar to that observed experimentally for completely wetting fluids on dry surfaces (Huppert 1982; Silvi & Dussan V. 1991; de Bruyn 1992). We also note that saw-tooth patterns corresponding to different δ values can be scaled into a single pattern when appropriately normalizing (3.7) by setting $\alpha \to (\chi/\omega)\alpha$, $\tau \to (\psi/\chi^2)\tau$ and $w \to (\psi/\chi)^{1/2}w$ to obtain the universal form

$$\alpha_\tau + \alpha_{ww} + \alpha_{wwww} + (\alpha\alpha_w)_w = 0.$$

The above observations indicate that the instability on a pre-wetted surface is distinctly different from the instability on a dry plane as was first discovered experimentally by Veretennikov *et al.* (1998). Consequently, we cannot expect δ to model wettability and contact line motion on a dry surface. The model used to remove the singularity associated with a contact line plays a secondary role in the linear stage of the instability (for the precursor film model this is the case when δ is small) but it becomes critical in the nonlinear stage. Consequently, a true contact angle boundary condition is necessary to obtain the two instability patterns seen experimentally depending on the wettability characteristics of the solid–liquid system. This is consistent with the numerical solution by Moyle, Chen & Homsy (1999) of the

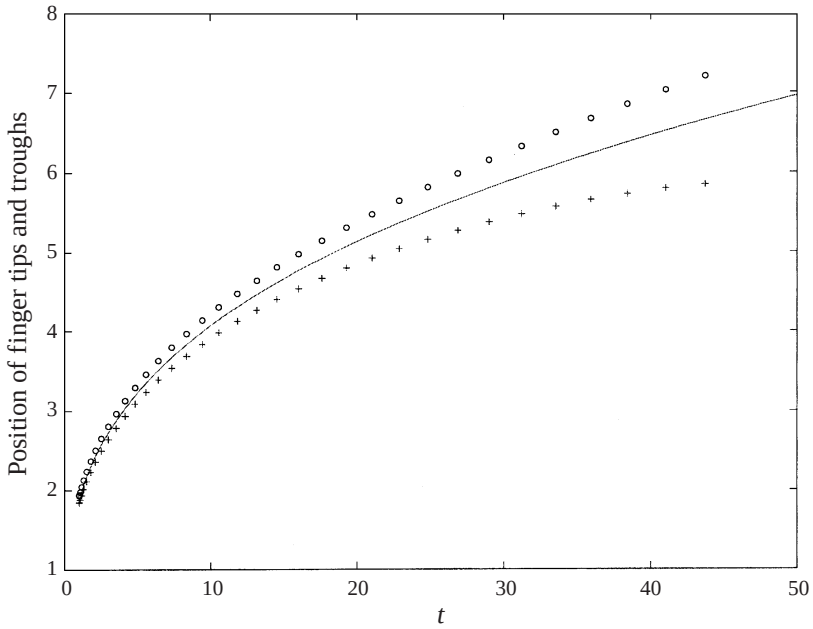

FIGURE 9. Front position versus time t for the conditions of figure 5. The open circles and crosses show the maxima and minima of the perturbed contact line respectively while the dashed line corresponds to Huppert's $t^{1/3}$ behaviour of the unperturbed front.

fully nonlinear moving boundary problem in (2.1) adopting a Navier-type slip model. However, Moyle *et al.* as well as Schwartz (1989) forced the growth of fingers by an appropriately chosen initial condition (corresponding to the most unstable wavelength according to linear theory for the study by Moyle *et al.*). The present study predicts the fingering pattern for perfectly wetting fluids and at the same time demonstrates that the wavelength selected by the system is the one predicted from linear stability analysis (see discussion below).

Figures 7 and 8 contrast the evolution with the experimental data by Veretennikov *et al.* for Castor oil spreading on a plane with an 8° inclination angle covered with a prewetting film of the same liquid. The authors are unable to measure the precursor film thickness and they use the drainage time as a qualitative measure for this thickness. Depending on the time of drainage they were able to produce uniform prewetted films of arbitrary δ. These are the only experiments available in the literature for prewetted planes and since the inclination angle is small and the value of δ unknown we do not make a qualitative comparison with experiments. Nevertheless, the shape of the contact line is in good agreement with the experimental data even though the extra term in the dimensional form of (2.1), $-\rho g \cos\beta (h^3 h_x)_x$, associated with the gravitational component in the direction perpendicular to the solid boundary has been neglected in our theory. Preliminary analysis shows that this term does not alter the functional form of (3.7) (as an inspection of the possible nonlinearities also indicates – see discussion in § 2); however, we anticipate that the value of the coefficients in (3.7) for the same δ will be different.

Figure 8(*a*) shows the temporal evolution of the contact line for $\delta = 0.1$ in an extended domain $L = 16L_m$ using appropriately smoothed random noise generated by a uniform distribution in the interval $[-0.1, 0.1]$ as initial condition. This small-

amplitude initial condition evolves into a series of 16 fingers with wavelength – measured between subsequent maxima – close to that predicted by the linear stability theory. When L is not an integer multiple of L_m the number of fingers seems to be equal to the integer immediately above or below L/L_m. Some of the fingertips are relatively flat while the minima between subsequent fingers are always sharp. A variation in speed and finger length is also observed with the longer fingers travelling faster. Some of the primary fingers are separated further than others with a relatively flat contact line in between for a sufficiently long time. These flat areas eventually break into rivulets (as the amount of liquid sucked from the minima by the primary fingers decreases as the length of these fingers increases and liquid accumulates at the minima leading to secondary fingers) with length smaller than the primary fingers and with one of the rivulets moving faster than the others. The equation blows-up before we can decipher the final evolution but a possible scenario could be that all these rivulets emerging out of flat areas between primary fingers are eventually combined into one single finger. In all cases the maxima move faster than the minima which slow down significantly at large times. Figure 9 shows the variation of the maxima and minima position versus time in the laboratory frame of reference for the evolution depicted in figure 5. Clearly both fingertips and minima follow the $t^{1/3}$ behaviour predicted by Huppert at early times. Eventually the maxima move faster than the unperturbed contact line and the minima slower without stopping completely. These observations are in quantitative agreement with existing experimental data of the fingering instability on dry surfaces (Huppert 1982; Silvi & Dussan V. 1991; Jerret & de Bruyn 1992). An interesting result concerning the nonlinear evolution in figure 5 is that the fingertip and trough positions are described very well by the power-law time-dependences $t^{0.35}$ and $t^{0.31}$ respectively with the average speed of tips and troughs being very close to $t^{1/3}$ at all times.

5. Summary and conclusion

We have analysed the nonlinear stage of the fingering instability problem introduced by Huppert. A constant-thickness precursor film was assumed ahead of the macroscopic front. Previous theory has dealt mainly with the linear stage of the instability and hence is only strictly valid for infinitesimal disturbances of a truly nonlinear system. It thus seems pertinent to develop a theory for the nonlinear regime. Using methods from dynamical systems, a partial differential equation for the evolution of the fingers in the weakly nonlinear stage of the instability was derived. The equation is accurate up to third order in the amplitude of the disturbances. The instability is a phase instability due to the translational symmetry of the system in the streamwise direction. The theory exploits the existence of a null eigenfunction associated with the translational invariance. We have shown through numerical experiments that the fingers develop a saw-tooth pattern qualitatively similar to that observed experimentally for completely wetting fluids on a dry surface. The fingers that developed are characterized by sharp minima and flat maxima. Interestingly, the parallel-sided fingers for partially wetting fluids on dry surfaces were never observed in our numerics. This implies that the precursor film model cannot be used to model spreading of partially wetting fluids on dry surfaces. Moreover, large values of the precursor film thickness correspond to a small number of fingers. In contrast, for spreading on a dry plane, we know from existing experimental data that the more wetting the fluid the larger the number of developed fingers. Hence, spreading on a pre-wetted surface seems to be distinctly different from spreading on dry surfaces. Finally, our numerical

experiments revealed that fingering can be prevented at large values of the precursor film thickness.

The analysis presented here is intended to provide a theoretical framework for the study of the nonlinear dynamics associated with the motion of forced contact lines. The approach we developed enables us to characterize the instability, demonstrate the wavelength selection process and describe the evolution after the onset. An important issue that should be resolved next is the presence of a true contact line. This will complicate the approach since the contact line advances in a direction normal to itself and the dynamic contact angle boundary condition must be applied in a direction normal to the contact line. Preliminary analysis indicates that (3.7) is replaced with a system of two coupled nonlinear partial differential equations for the height of the front and location of the contact line boundary respectively.

The author is grateful to Professor G. M. Homsy for helpful comments on the manuscript, Professor H.-C. Chang for numerous stimulating discussions on pattern formation and nonlinear dynamics, and would also like to thank the University of Leeds for providing the computing facilities to perform the numerical work in this study.

REFERENCES

Bertozzi, A. L. & Brenner, M. P. 1997 Linear stability and transient growth in driven contact lines. *Phys. Fluids* **9**, 530–539.

Bruyn, J. R. de 1992 Growth of fingers at a driven three-phase contact line. *Phys. Rev.* A **46**, R4500–R4503.

Carr, J. 1981 *Applications of Center Manifold Theory*. Springer.

Chang, H.-C. 1989 Onset of nonlinear waves on falling films. *Phys. Fluids* A **1**, 1314–1327.

Chang, H.-C. 1994 Wave evolution on a falling film. *Ann. Rev. Fluid Mech.* **26**, 103–136.

Chang, H.-C. & Demekhin, E. A. 1996 Solitary wave formation and dynamics on falling films. *Adv. Appl. Mech.* **32**, 1–58.

Chang, H.-C., Demekhin, E. A. & Kopelevich, D. I. 1995 Stability of a solitary pulse against wave packet disturbances in an active medium. *Phys. Rev. Lett.* **75**, 1747–1750.

Chang, H.-C., Demekhin, E. A. & Kopelevich, D. I. 1996 Local stability theory of solitary pulses in an active medium. *Physica* D **97**, 353–375.

Cheng, M. & Chang, H.-C. 1990 A generalized sideband stability theory via center manifold projection. *Phys. Fluids* A **2**, 1364–1379.

Conte, S. D. 1966 The numerical solution of linear boundary value problems. *SIAM Rev.* **8**, 309–321.

Dussan V., E. B. 1979 On the spreading of liquids on solid surfaces: static and dynamic contact lines. *Ann. Rev. Fluid Mech.* **11**, 371–400.

Dussan V., E. B. & Davis, S. H. 1974 On the motion of a fluid-fluid interface along a solid surface. *J. Fluid Mech.* **65**, 71–103.

Elphick, C., Ierley, G. R., Regev, O. & Spiegel, E. A. 1991 Interacting localised structures with Galilean invariance. *Phys. Rev.* A **44**, 1110–1122.

Fauve, S. 1987 Large scale instabilities of cellular flows. In *Instabilities and Nonequilibrium Structures* (ed. E. Tirapegni & O. Villaroel), pp. 63–88. D. Reidel.

Fraysse, N. & Homsy, G. M. 1994 An experimental study of rivulet instabilities in centrifugal spin coating of viscous newtonian and non-newtonian fluids. *Phys. Fluids* **6**, 1491–1504.

Fujimura, K. 1991 Methods of center manifold and multiple scales in the theory of weakly nonlinear stability of fluid motions. *Proc. R. Soc. Lond.* A **434**, 719–733.

Gallay, T. 1993 A center-stable manifold theorem for differential equations in Banach spaces. *Commun. Math. Phys.* **152**, 249–268.

Gennes, P. G. de 1985 Wetting: statics and dynamics. *Rev. Mod. Phys.* **57**, 827–863.

Goodwin, R. & Homsy, G. M. 1991 Viscous flow down a slope in the vicinity of a contact line. *Phys. Fluids* A **4**, 515–528.

Guckenheimer, J. & Holmes, P. 1983 *Nonlinear Oscillations, Dynamical Systems and Bifurcations of Vector Fields*. Springer.

Haley, P. J. & Miksis, M. J. 1991 The effect of the contact line on droplet spreading. *J. Fluid Mech.* **223**, 57–81.

Hocking, L. M. 1990 Spreading and instability of a viscous fluid sheet. *J. Fluid Mech.* **211**, 373–392.

Hocking, L. M. 1992 Rival contact angle models and the spreading of drops. *J. Fluid Mech.* **239**, 671–681.

Homsy, G. M. 1974 Model equations for wavy viscous film flow. *Lectures in Applied Mathematics*, **15**, pp. 191–194. Springer.

Huh, C. & Scriven, L. E. 1971 Hydrodynamic model of steady movement of a solid/liquid/fluid contact line. *J. Colloid Interface Sci.* **35**, 85–101.

Huppert, H. E. 1982 Flow and instability of a viscous current down a slope. *Nature* **300**, 427–429.

Jerret, J. M. & Bruyn, J. R. de 1992 Fingering instability of a gravitationally driven contact line. *Phys. Fluids* A **4**, 234–242.

Kalliadasis, S. & Chang, H.-C. 1994*a* Apparent dynamic contact angle of an advancing gas-liquid meniscus. *Phys. Fluids* **6**, 12–23.

Kalliadasis, S. & Chang, H.-C. 1994*b* Drop formation during coating of vertical fibres. *J. Fluid Mech.* **261**, 135–168.

Kalliadasis, S. & Chang, H.-C. 1996 Dynamics of liquid spreading on solid surfaces. *Indust. Engng. Chem. Res.* **35**, 2860–2874.

Kuramoto, Y. 1984 *Chemical Oscillations, Waves and Turbulence*. Springer.

Lin, S. P. 1974 Finite amplitude side-band stability of a viscous film. *J. Fluid Mech.* **63**, 417–429.

Melo, F., Joanny, J. F. & Fauve, S. 1989 Fingering instability of spinning drops. *Phys. Rev. Lett.* **63**, 1958–1961.

Mercer, G. N. & Roberts, A. J. 1990 A centre manifold description of contaminant dispersion in channels with varying flow properties. *SIAM J. Appl. Maths* **50**, 1547–1565.

Moriarty, J. A., Schwartz, L. W. & Tuck, E. O. 1991 Unsteady spreading of thin liquid films with small surface tension. *Phys. Fluids* A **3**, 733–742.

Moyle, D. T., Chen, M.-S. & Homsy, G. M. 1999 Nonlinear rivulet dynamics during unstable dynamic wetting flows. *Intl. J. Multiphase Flow* **25**, 1243–1262.

Nepomnyaschy, A. A. 1974 Stability of wave regimes in a film flowing down an inclined plane. *Izv. Akad. Nauk SSSR, Mekh. Zhidk Gaza* **3**, 28–34.

Roberts, A. J. 1988 The application of center manifold theory to the evolution of systems which vary slowly in space. *J. Austral. Math. Soc.* B **29**, 480–500.

Schwartz, L. W. 1989 Viscous flow down an inclined plane: instability and finger formation. *Phys. Fluids* A **1**, 443–445.

Schwartz, L. W. & Eley, R. R. 1998 Simulation of droplet motion on low-energy and heterogeneous surfaces. *J. Colloid Interface Sci.* **202**, 173–188.

Shikhmurzaev, Y. D. 1997 Moving contact lines in liquid/liquid/solid systems. *J. Fluid Mech.* **334**, 211–249.

Shkadov, V. Ya 1973 Some methods and problems in hydrodynamic stability theory. *Inst. of Mech. of Moscow State Univ., Proc.* 25 (in Russian).

Silvi, N. & Dussan V., E. B. 1985 On the rewetting of an inclined solid surface by a liquid. *Phys. Fluids* **28**, 5–7.

Spaid, M. 1995 An investigation of newtonian and viscoelastic dynamic contact lines. PhD thesis, Stanford University.

Spaid, M. & Homsy, G. M. 1996 Stability of newtonian and viscoelastic dynamic contact lines. *Phys. Fluids* **8**, 460–478.

Teletzke, G. F., Davis, H. T. & Scriven, L. E. 1988 Wetting hydrodynamics. *Revue Phys. Appl.* **23**, 989–1007.

Troian, S., Herbolzheimer, E., Safran, S. & Joanny, J. 1989 Fingering instabilities of driven spreading films. *Europhys. Lett.* **10**, 25–30.

Tuck, E. O. & Schwartz, L. W. 1990 A numerical and asymptotic study of some third-order ordinary differential equations relevant to draining and coating flows. *SIAM Rev.* **32**, 453–469.

Veretennikov, I., Indeikina, A. & Chang, H.-C. 1998 Front dynamics and fingering of a driven contact line. *J. Fluid Mech.* **373**, 81–110.